A Virtual Resistance Optimization Method Based on Hybrid Index in Low-Voltage Microgrid

Yifei Yin[1] | Xinwei Yu[2]

[1]Department of Electrical Information,Shandong University of science and technology,China.

[2]Department. of Electrical Engineering,China university of petroleum(east China),China.

Correspondence

Yifei Yin, department of Electrical information,Shandong University of science and technology, NO.579 Qianwangang Road, Huangdao District, Qingdao City, Shandong Province, China.Email:1250279987@qq.com

Abstract

The introduction of virtual resistance can effectively suppress the circulating current between microsources and improve power allocation in low-voltage microgrid, but it also causes the voltage deviation of microsources' inverters. An optimization method of virtual resistance based on hybrid index is proposed in order to suppress circulating current and improve voltage deviation at the same time in this paper. The gradient descent method is used to design the virtual resistance optimization process, aiming at the optimization of hybrid index composed of circulating current and voltage deviation. The constraints are deduced with power quality requirements, capacity limitation and static stability, and then virtual resistance values are optimized. The effects of switching load and microsource on the optimization results are analyzed through the simulation of low-voltage microgrid, and the simulation results show that the virtual resistance optimization method can significantly suppress circulating current while improving power quality.

Keywords Low-voltage microgrid · Virtual resistance optimization · Circulating current suppression · Voltage deviation · Hybrid index

1 | Introduction

Microgrid is a small power generation and distribution system which integrates distributed generators, load, energy storage equipment, converter and monitoring protections [1-2]. When distributed generators are connected to utility grid through inverters and feeders, differences in feeder parameters and inverter control strategies easily cause circulating current and uneven power distribution among micro-sources. The serious circulating current causes power oscillation and even system collapse, and uneven power distribution causes long-term insufficient output of some micro-sources in the system with a large number of micro-sources [3]. Improvements to the control of inverters are investigated in relevant literatures in order to solve the above problems, and the introduction of virtual impedance is a typical improvement method.

The design of virtual impedance is generally based on feeder Impedances and droop-control curves of different voltage levels. The traditional P-f and Q-V droop control does not meet system characteristics because of the large resistive component of the feeder impedance in the low-voltage microgrid. The existing virtual impedance design methods can be divided into two categories according to whether the droop characteristic curve is improved. It is commom to adopt the P-f and Q-V droop controller and design a virtual inductor in order to change the impedance ratio, which make it inductive to meet traditional droop characteristics. Zhu Y et al. adopt virtual reactance to improve the resistance-inductance ratio, and the output active power is adopted to modify the virtual resistance to achieve the purpose of optimal distribution of active power [4]. Zhu G et al. introduce virtual reactance to increase the overall reactance value, and the deviation between inverter voltage and bus voltage is introduced into the Q-V droop characteristic curve to improve the allocation accuracy of reactive power [5]. Wen C et al. propose a virtual impedance control method based on dq conversion, and verify that the application of virtual impedance can effectively suppress the circulating current [6-7]. Cai H et al. propose the metod of virtual negative impedance, which adopts negative virtual resistance to make the overall impedance inductive and improve the accuracy of power decoupling [8]. Hoang et al. obtain the average output power based on the droop coefficient of each inverter, and realize the output power share control of micro-sources [9]. The other researchers adopt P-V and Q-f droop controller and

designing a virtual resistor to improve power allocation. Fixed virtual resistors are adopted to verify the effectiveness of the proposed method for circulating current suppression [10]. Dou C et al. propose a method of adjusting virtual resistance value with active power to suppress circulating current and improve power decoupling accuracy at the same time [11]. In summary, the circulating current can be suppressed and the active and reactive power can be reasonably distributed by reasonably designing virtual impedance.

Virtual impedance has the characteristics of high flexibility and no power loss, but it can cause static voltage deviation. Therefore, many scholars have carried out research on the improvement methods of voltage deviation. Zhang H et al. propose to improve voltage quality by adjusting virtual resistance and virtual reactance with reactive power, but it requires high reliability of communication between micro-sources[12]. Zhang Y et al. introduce the output voltage of the inverter into the droop control loop or voltage loop, which reduces the voltage drop caused by virtual impedance to a certain extent [13-14]. Han Hua et al. proposes a voltage recovery mechanism, which means that voltage compensation is performed immediately when voltage drop is detected [15]. However, the selection of compensation deviation lacks reasonable basis, and the timeliness can not be reliably guaranteed. Xia Y et al adopt double-loop controller instead of traditional three-loop controller, and improve voltage deviation by reasonably designing virtual resistance[16]. Augustine S et al propose a method of adjusting virtual resistance by feeder impedance and micro-source capacity and verify its effectiveness in reducing voltage deviation[17-18]. Peng Z et al. apply an intelligent optimization algorithm to find the optimal parameters to ensure that the frequency and voltage change and rate of change are minimal in the transient process[19]. Wang et al. propose the consensus algorithm to achieve the frequency adjustment and improve the distribution accuracy of active power[20-21]. It can be seen that the existing research generally improves the voltage quality by adjusting the droop characteristic curve or adding new controllers and control mechanisms, but the above methods do not coordinate the design of improving the voltage quality, suppressing circulation current and improving the power sharing, which fails to achieve the coordinated control effect of suppressing the circulation current and improving the voltage quality.

In this paper, the value of virtual resistance is optimized by optimizing the hybrid index based on circulating current and voltage deviation, so that the performance of the system can reach an optimal state in the contradiction between power allocation and voltage deviation. In addition, the design of the virtual resistance meets the system operation constraints and static stability requirements. It further limits the value range of virtual resistance and ensures that the virtual resistance can be adjusted quickly until the optimal value is obtained. The virtual resistance optimization design method is compared with other design methods in the simulation of low-voltage microgrid with multi-sources, which verifies the effectiveness of the optimization design in improving the quality of micro-source voltage and significantly suppressing the circulating current.

2 | Photovoltaic System

The introduction of virtual resistance aims at suppressing circulating current and improving power allocation, but it also causes output voltage deviation. Therefore, the hybrid index is selected to optimize the design of virtual resistance by combining these two factors. In this section, the selection of hybrid index and the derivation of its mathematical model are elaborated, the corresponding relationship between mixing index and virtual resistance is analyzed, and the design basis of weighting factor of hybrid index is designed.

2.1 | Selection of hybrid index

An islanded low-voltage microgrid can be regarded as a system of parallel micro-sources, and its circulating current can be analyzed according to the circulating current of the inverter parallel system [22]. There are differences in the definition of circulating current in different literatures, but the definitions in [23] are identical and widely used, which can be derived as:

$$I_{\mathrm{h}}=\frac{I_{\mathrm{DG1}}-I_{\mathrm{DG2}}}{2} \tag{1}$$

where I_{h} is the circulating current between the micro-source DG_1 and DG_2. In the system with a large number of micro-sources, the circulating current of the nth micro -source is defined as:

$$I_{\mathrm{h}n}=\left|I_{\mathrm{avg}}-I_{\mathrm{DG}n}\right| \tag{2}$$

where I_{avg} is the RMS of all the micro-source output currents in the system and $I_{\mathrm{DG}n}$ is the RMS of the nth micro-source output current. Three-phase symmetric

feeders and loads are adopted in this paper and therefore the RMS of single-phase micro-source output current is adopted as I_{avg}.

The voltage deviation refers to the static voltage deviation caused by the introduction of virtual resistance. The product of the output current of the micro-source and the virtual resistance is used as the adjustment of the reference value in the outer loop voltage, which is as follows.

$$\begin{cases} U_{\alpha \mathrm{ref}} = U_{\alpha}^{*} - R_{\mathrm{v}} \cdot I_{\mathrm{DG}\alpha} \\ U_{\beta \mathrm{ref}} = U_{\beta}^{*} - R_{\mathrm{v}} \cdot I_{\mathrm{DG}\beta} \end{cases} \tag{3}$$

where R_v is the value of virtual resistance and the voltage drop is the deviation between the voltage reference value and the actual voltage reference value. And the expression above is in stationary reference frame. Based on the analysis, the voltage deviation of the nth micro-source can be expressed as:

$$U_{\mathrm{v}n} = \left| R_{\mathrm{v}n} \cdot I_{\mathrm{DG}n} \right| \tag{4}$$

The concept of hybrid index is proposed based on the analysis above and the hybrid index of the nth micro-source is defined as:

$$T_n = T_{\mathrm{h}} + T_{\mathrm{v}} = k_1 \left(I_{\mathrm{avg}} - I_{\mathrm{DG}n} \right)^2 + k_2 \left(R_{\mathrm{v}n} \cdot I_{\mathrm{DG}n} \right)^2 \tag{5}$$

where k_1 and k_2 are the weight factors of circulating current and voltage deviation in the hybrid index respectively. The two weight factors are not comparable in the unit, so they need to be designed reasonably and the design principles are shown in Section 2.3.

The increase of circulating current reflects the increase of circulating current between the micro-source and all other micro-sources, corresponding to the increase of hybrid index. When the capacity and the control of the inverters are the same, the circulating current can reach the minimum value of zero in theory, which means there is no circulating current among micro -sources. The larger the voltage deviation is, the larger the voltage drop caused by the virtual resistance and the hybrid index are. Therefore, the hybrid index can reflect the comprehensive effect of circulating current and voltage deviation.

2.2 | Hybrid Index Mathematical Model

The micro-source and its inverter are equivalent to the Thevenin model, as shown in Figure 1. The equivalent impedance of the inverters and loads near inverters are neglected in the low-voltage microgrid topology.

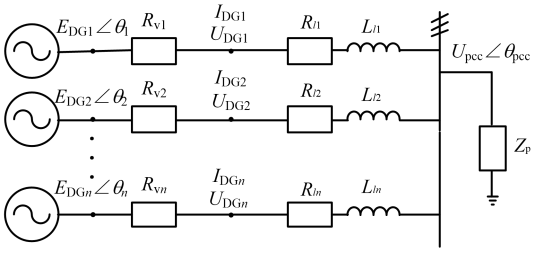

FUGURE 1 Frame diagram of low-voltage microgrid

As can be seen from Figure 1, the current and voltage equations are as follows.

$$\sum_{j=1}^{n} I_{\mathrm{DG}j} - U_{\mathrm{pcc}} \angle \theta_{\mathrm{pcc}} / Z_{\mathrm{p}} = 0 \tag{6}$$

$$I_{\mathrm{DG}n} = \frac{E_{\mathrm{DG}n} \angle \theta_n - U_{\mathrm{pcc}} \angle \theta_{\mathrm{pcc}}}{R_{\mathrm{v}n} + R_{ln} + jX_{ln}} \tag{7}$$

When the capacity and the control of the inverters are the same, the $E_{DG}\angle\theta$ is approximately equal. In addition, R_{l1} is much larger than L_{l1} in the impedance of the low-voltage feeder. Therefore, the hybrid index of the nth micro-source is expressed as:

$$T_n = N^2 \left(k_1 O_n^2 + k_2 R_{\mathrm{v}n}^2 M_n^2 \right) \tag{8}$$

where

$$\begin{cases} N = \dfrac{E_{\mathrm{DG1}}}{Z_{\mathrm{p}}} / \left(\dfrac{1}{Z_{\mathrm{p}}} + \sum\limits_{j=1}^{n} M_j \right) \\ M_n = 1/(R_{\mathrm{v}n} + R_{ln}) \\ O_n = \dfrac{1}{n} \sum\limits_{j=1}^{n} M_j - M_n \end{cases} \tag{9}$$

When the virtual resistance of the nth micro-source is analyzed, it is assumed that virtual resistances of all other micro-sources are constant. As shown in Equation (8), when loads and feeders are fixed and the weight factors k_1 and k_2 are selected, T_n is related to the unique variable R_{vn}. Assuming that the feeder resistance of DG_1 is 0.1Ω; the feeder resistance and the virtual resistance of DG_2 are both 0.2Ω in the low-voltage microgrid with two micro-sources, the correspondence between T_1 and R_{v1} is shown in Figure 2.

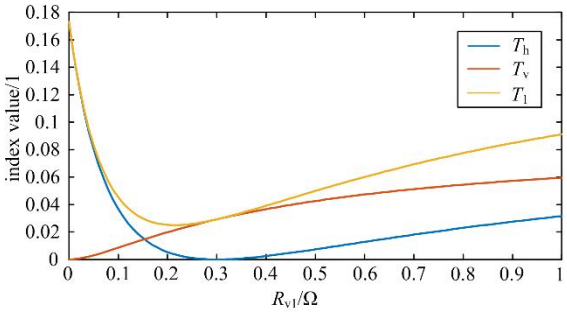

FIGURE 2 Diagram of the correspondence between virtual resistance and hybrid index

As can be seen from Figure 2, when the sum of R_{v1} and R_{l1} is equal to the sum of R_{v2} and R_{l2} in the process of R_{v1} increasing, which means R_{v1} is 0.3Ω, the circulation index T_h reaches the minimum of 0. However, the voltage drop caused by the virtual resistance increases gradually, and the voltage deviation index T_v increases continuously. Therefore, T_1 decreases first and then increases. That is, there is a unique value of the virtual resistance making the hybrid index minimize. Considering that the feeder reactance of the micro-source, the virtual resistance corresponding to the minimum value of the hybrid index is approximately equal to the resistance difference.

2.3 | weight factor

There is no comparability between two weight factors' units for k_1 corresponding to T_h, whose unit is A^2,and k_2 corresponding to T_v, whose unit is V^2. Therefore, the values of k_1 and k_2 is different from that of the typical weight factors, of which the units are the same and the values are from 0 to 1. Two weighting factors are designed based on the analysis above.

Virtual resistances are introduced in all inverters' control in the low-voltage microgrid, so the first inverter is taken as an example to describe the value design processes of k_1 and k_2 in the hybrid index T_1. All virtual resistors except R_{v1} are taken as constants in the weight factor design of T_1. From Equation (8), the optimal value of R_{v1} corresponding to the extreme point of T_1 is as follows.

$$R_{v1z}=\frac{\left(n-1-R_{l1}X\right)Y}{\frac{k_2}{k_1}\left(1+\frac{R_{l1}}{Z_p}+R_{l1}X\right)+YX} \tag{10}$$

where

$$\begin{cases} X=\sum_{j=2}^{n}M_j \\ Y=\dfrac{n-1+nZ_pX}{n^2Z_p} \end{cases} \tag{11}$$

The value of R_{v1z} is negatively correlated with the ratio of k_2 to k_1 in Equation (10). It must be noted that, Equation (10) is only used to analyze the first inverter, and cannot be used to acquire the global optimum solution of the virtual resistance R_{v1}. Assuming that the feeder resistances of DG_1 and DG_2 are 0.1Ω and 0.4Ω respectively in the low-voltage microgrid with two micro-sources, the correspondence between the ratio of k_2 to k_1 (set as k_b) and R_{v1z} is shown in Figure 3.

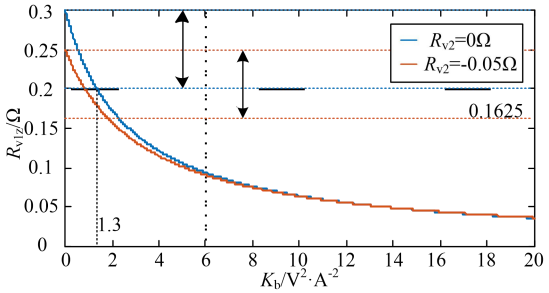

FIGURE. 3 Correspondence diagram of weight factor ratio and optimum value of virtual resistance

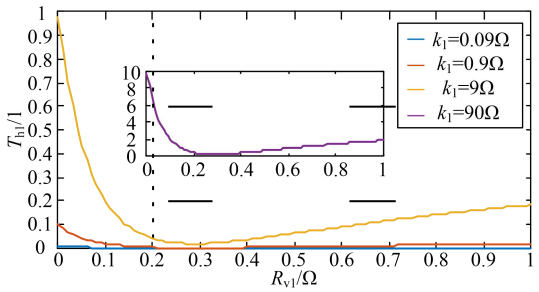

FIGURE 4 Diagram of the correspondence between virtual resistance and hybrid index

In order to ensure that the value of R_{v1z} can basically achieve accurate power allocation , the value range of R_{v1z} is as follows.

$$\frac{3}{4}\left(R_{v2}+R_{l2}\right)-R_{l1}\le R_{v1z}\le R_{v2}+R_{l2}-R_{l1} \tag{12}$$

According to Equation (12), k_b ranges from 0 to 1.3 in Figure 3. When the R_{v2} value is negative, its variation does not affect the lower bound of k_b, so the value range of k_b includes the negative value of the virtual resistance. The smaller the k_b value is, the larger the proportion of circulating current in the hybrid index is, which means that the power allocation degree is more important in the

balance between suppressing circulating current and reducing voltage deviation. Similarly, the larger the k_b value is, the more important the voltage quality is. When k_b is 0.2, the relationship between the weight factor and the hybrid index is as shown in Figure 4.

As shown in Figure 4, the small value of k_1 makes the hybrid index small, which increases the difficulty of optimization convergence. k_b ranges from 1 to 100 in order to reduce the difficulty of convergence.

$$\begin{cases} 0 \le k_2 / k_1 \le 1.3 \\ 1 \le k_1 \le 100 \end{cases} \tag{13}$$

3 | Optimum Design Method of Virtual Resistance

The gradient descent method is used to optimize the virtual resistance with the objective of optimizing the hybrid index. The process of virtual resistance optimization, constraints and convergence are described in detail.

3.1 | Optimizing process

The gradient descent method is applied to optimize the virtual resistance, and the iteration formula of the virtual resistance is as follows.

$$\frac{dR_{vn}}{dt} = -\alpha \cdot \text{sign}(\frac{dT_n}{dR_{vn}}) \cdot e^{kt} \tag{14}$$

where α is the learning rate and a positive constant; k is the attenuation coefficient and a negative constant. Both of them need to be reasonably designed to avoid non-convergence. In addition, the convergence condition in the iteration process is as follows.

$$\left| dT_n / dt \right| \le \varepsilon \tag{15}$$

According to the iteration algorithm above, taking the micro-source DG_1 as an example, the overall flow chart of the virtual resistance optimization is as shown in Figure 5.

As shown in Figure 5, the R_{v1} optimization process needs R_{v1} and T_1 as the input to start the iteration. T_1 is calculated by the current I_{DG1} through local measurements and the output current of all other inverters transmitted by the communication line, which depends on the highly-reliable communication line. In case of communication failure, T_1 only acquires the local current I_{DG1}, which results in the optimization value of R_{v1} being 0. In case of communication delay, the delay effect is equivalent to the corresponding feeder length decreasing, which leads to a larger optimization value. This indicates that the communication problem affects the accuracy of the optimization results.

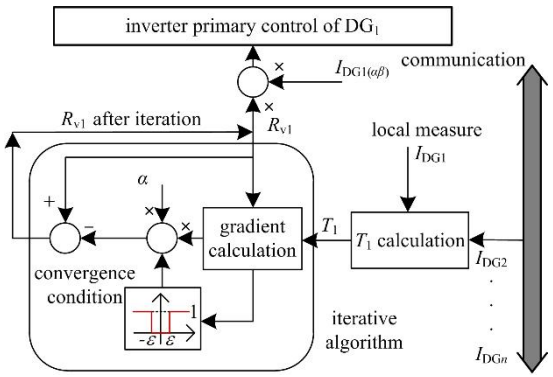

FIGURE. 5 Flow diagram of iteration algorithm

Compared with other peer-to-peer control based on the voltage and current transmitted by the communication line, the iteration process proposed only needs current, which reduces the transmission volume of communication lines and alleviates the pressure of communication transmission. In general, solving T_1 and iterating are regarded as the secondary control of the inverters. The optimization value of R_{v1} is entered into the primary control to realize the hierarchical control of the inverters.

3.2 | Constraint Condition

The constraints in the virtual resistance optimization process include the power quality requirements of micro -sources, the capacity limitation of the inverters and the static stability requirements. The power quality of the low-voltage microgrid includes voltage deviation, voltage harmonics and frequency allowable deviation. Three-phase symmetrical load is adopted, so three-phase unbalance is not considered. Voltage harmonics are constrained by the design of QPR controller in primary control of inverters, and frequency allowable deviation is constrained by the design of droop coefficient in the droop control. Therefore, voltage deviation and power angle limitation are described in detail, and the rests of power quality requirements are not elaborated.

The allowable fluctuation range of three-phase voltage in low-voltage microgrid is ±7%, corresponding to the limit range of U_{pcc} in Figure 1. In addition, there is

the maximum power angle deviation between the output voltage of the micro-source inverter and U_{pcc}. Considering the symmetry of three-phase load and three-phase line parameters, the single-phase constraints of the nth micro-source are obtained based on the constraints above.

$$\begin{cases} (1-7\%) \le U_{pcc}^{*} \le (1+7\%) \\ 0 \le \theta_n - \theta_{pcc} \le \theta_{max} \end{cases} \tag{16}$$

In addition, the output power P and Q of the micro-source inverters are limited by the capacity of the inverters, which are expressed as:

$$\begin{cases} P_n \le P_{max} \\ Q_n \le Q_{max} \end{cases} \tag{17}$$

where, P_n and Q_n are calculated from the output power of the nth micro-source, whose specific expressions can be found in reference [8]. The impedance, appearing in the expression of P_n and Q_n, includes the equivalent output impedance, the feeder impedance and the virtual resistance. Equation (16-17) are virtual resistance constraints based on the power quality constraint and the inverter capacity limitation. Assuming that the maximum power angle deviation is 10 degrees and the maximum power limit is 20 kW and 10 kvar, the permissible range of R_{vn} is shown in Figure 6.

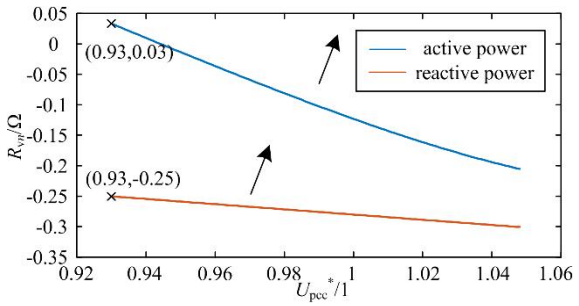

FIGURE 6 Diagram of bus voltage and permissible range of virtual resistance

As shown in Figure 6, the range of virtual resistance gradually increases with the increase of bus voltage, corresponding to the range of arrow pointing. The closer the bus voltage is to the equivalent voltage of the micro-source, the more difficult it is for the output active power to reach the limit value. Therefore, the allowable virtual resistance range increases with the bus voltage increasing. In order to ensure that the power constraints are satisfied within the allowable voltage fluctuation range, the minimum allowable range is taken as the value range of the virtual resistance, corresponding to the virtual resistance with a lower limit of 0.03Ω in Figure 6. It should be noted that there is also an upper limit constraint on voltage phase angle θ_n besides bus voltage fluctuation. The simulation results show that the phase angle has little influence on the virtual resistance, so the voltage phase angle is not used as a variable but a constant.

The method of judging the small signal stability is the small signal analysis of the inverter output equation. The droop characteristic and output power characteristic can be linearized when small interference occurs in equilibrium state, which is expressed as:

$$\begin{cases} \Delta E_{DG} = -k_e \Delta P \\ \Delta f = k_f \Delta Q \\ \Delta P = k_1 \Delta E_{DG} + k_2 \Delta\theta \\ \Delta Q = k_3 \Delta E_{DG} + k_4 \Delta\theta \end{cases} \tag{18}$$

where k_e and k_f are the droop coefficients of P-V and Q-f droop characteristic curves, which can be designed based on the output power limit and power quality requirements of the inverters. k_1, k_2, k_3 and k_4 are variables including virtual resistance and line parameters, which can be derived from the partial derivative of the output power equation of the micro-source, shown in Figure 1. Consequently,

$$s^3\Delta\theta + As^2\Delta\theta + Bs\Delta\theta + C\Delta\theta = 0 \tag{19}$$

where

$$\begin{cases} A = \omega_f (k_e k_1 + 2) \\ B = \omega_f (\omega_f + \omega_f k_e k_1 - 2\pi k_f k_4) \\ C = -2\pi k_f \omega_f^2 (k_4 + k_e k_1 k_4 - k_e k_2 k_3) \end{cases} \tag{20}$$

where ω_f is the cut-off frequency of the low-pass filter and a constant. Therefore, the small interference stability of micro-sources can be judged by the characteristic equation. In order to ensure good small interference stability, all real parts of the eigenvalue of Equation (19) should satisfy:

$$\mathrm{Re}(root) \le -k_r \tag{21}$$

where k_r is a positive constant.

Tab.1 Table of system parameters

system parameter	value
k_e/kV·MW^{-1}	0.25
k_f/Hz·Mvar^{-1}	0.667
ω_f/rad·s^{-1}	62.83
k_r/1	2.5

By substituting the parameters in Table 1 into the small disturbance stability constraint Equation(21), The

root locus diagrams under different virtual resistances is shown in Figure 7. The characteristic equation corresponds to three real roots. The values of $root_1$ and $root_3$ are always very small, which have little influence on the stability. $root_2$ gradually approaches 0 with the increase of R_{vn}, and has great influence on the stability of small interference. When the virtual resistance increases, the value of $root_2$ approximates to zero, and the static stability becomes worse. As shown in Figure 7, the virtual resistance should be less than 0.67Ω in order to satisfy the stability constraints, which means that there is an upper limit for the virtual resistance. It should be noted that the value of k_r affects the upper limit of virtual resistance due to the fluctuation of subjective factors. Considering that the optimal value of virtual resistance is basically less than half of 0.67Ω, it will not affect the final result of the virtual resistance optimization.

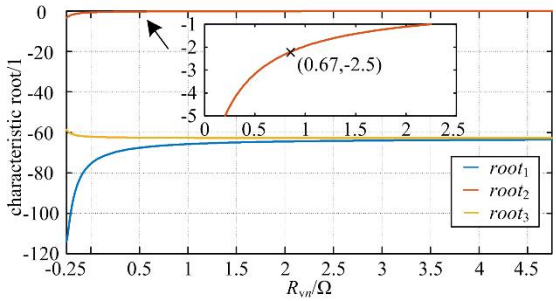

FIGURE 7 Root locus plot with different virtual resistances

The value range of the virtual resistance is obtained by analyzing the constraints of power quality, capacity constraints and small disturbance stability constraints, which is in favor of reducing the impact of initial iteration values and ensuring the fast convergence.

3.3 Optimal Convergence

According to the optimization process of the virtual resistance, the convergence analysis of the hybrid index in the iteration process is carried out. The hybrid index T_1 of the first micro-source is a function about independent variables R_{v1}, R_{v2}... R_{vn} in the low-voltage microgrid with many micro-sources. Therefore, the derivation of T_1 is as follows.

$$\frac{dT_1}{dt} = -\alpha e^{kt}\left[\frac{dT_1}{dR_{v1}}\mathrm{sign}\left(\frac{dT_1}{dR_{v1}}\right)+\frac{dT_1}{dR_{v2}}\cdot \mathrm{sign}\left(\frac{dT_2}{dR_{v2}}\right)+\cdots+\frac{dT_1}{dR_{vn}}\mathrm{sign}\left(\frac{dT_n}{dR_{vn}}\right)\right] \tag{22}$$

where

$$\frac{dT_1}{dR_{vj}} = \begin{cases} 2M_j^2N^2\left[k_1O_1\left(\dfrac{NO_1Z_p}{E_{DG1}}+\dfrac{n-1}{n}\right)+ k_2M_1R_{v1}\left(\dfrac{M_1NZ_pR_{v1}}{E_{DG1}}+R_{l1}\right)\right], j=1 \\ 2M_j^2N^2\left[k_1O_1\left(\dfrac{NO_1Z_p}{E_{DG1}}-\dfrac{1}{n}\right)+ k_2NM_1^2R_{v1}^2\dfrac{Z_p}{E_{DG1}}\right], j\neq 1 \end{cases} \tag{23}$$

If the sum of all the items on the right side of Equation (22) is positive, there exists a negative derivative for the hybrid index. It means that increasing the virtual resistance can ensure the hybrid index is close to the optimal value. The best value of iteration convergence is the virtual resistance value corresponding to that Equation (22) is 0. Therefore, the virtual resistance optimal value of the first micro-source is the R_{v1} corresponding to that Equation (22) is 0. The optimum virtual resistance of other micro-sources can be determined by the same process. Assuming that the feeder resistances of two micro-sources are 0.1Ω and 0.4Ω respectively in the low-voltage microgrid with two micro-sources, the convergence of the hybrid indexes T_1 and T_2 affected by virtual resistors is shown in Figure 8.

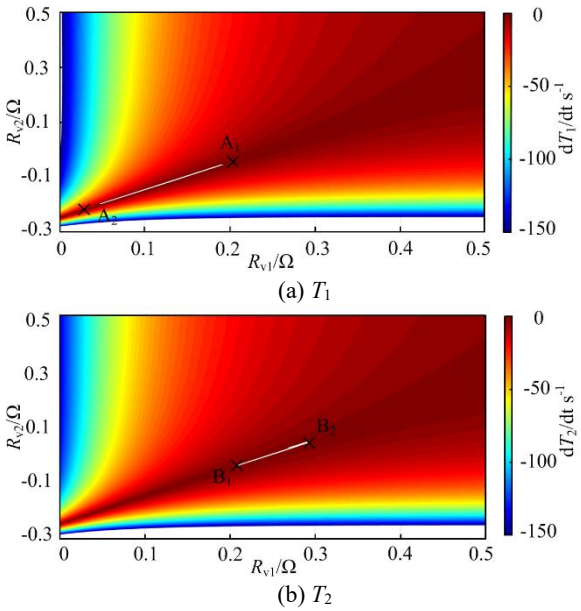

(a) T_1

(b) T_2

FIGURE 8 Convergence diagram of hybrid index

The white areas from A_1 to A_2 and from B_1 to B_2 correspond to that the convergence condition is greater than 0 in Figure 8. In Figure 8(a), both A_1 (0.21, -0.05, 0)

and A_2 (0.04, -0.27, 0) satisfy the convergence condition of 0, which corresponds to the minimum of the hybrid index. Corresponding to the point A_2 which satisfies the convergence condition, R_v is basically equal to the line impedance, so the voltage deviation caused by R_v does not meet the original design purpose, and the constraints described in the previous section can also avoid the virtual resistance converging to the point A_2.Therefore, the virtual resistance value corresponding to A_1 is the only optimal value satisfying the constraints. In Figure 8(b), The point B_2 (0.29, 0.05, 0) is similar to A_2, which means the best value satisfying the constraints is only the point B_1 (0.22, -0.06, 0).

In conclusion, the optimal convergence values A_1 and B_1 after the iteration of T_1 and T_2 corresponds to R_v ,which are unique and basically consistent, and the two virtual resistors are 0.21Ω and -0.05Ω respectively. This shows that the optimization process of the virtual resistance can converge to the only optimal value in the dual micro-source system.

4 | Simulation analysis of virtual resistance optimization

The simulation model of the low-voltage microgrid with micro-sources is built to analyze the effect of virtual resistance optimization. The simulation structure of the 0.4kV islanding microgrid is shown in the appendix.

Tab.2 System parameters used for simulation

system parameter	value
U_{dc}/kV	0.8
R_{f1}+jX_{f1}/Ω	0.6+j0.078
R_{f2}+jX_{f2}/Ω	0.9+j0.117
R_{f3}+jX_{f3}/Ω	0.7+j0.091
P+jQ/MVA	0.5+j0.3
L_f/mH、C_f/μF	0.5、150
k_{p1}、k_{p3}/1	0.8、0.8
k_{r1}、k_{r3}/1	50、20
k_p/1、t_f/s	0.6、1.2
k_1/kA^{-1}、k_2/kV^{-1}	9、1
k/s^{-1}、α/Ω^2	-0.009、0.006
ε/s^{-1}	0.005

Some of the control parameters are shown in Table 1 and the other system parameters are shown in Table 2. Specific design principles of the filter inductance and the filter capacitance can be found in reference [24]. Design principles of droop control coefficients can be found in reference [25]. Design principles of of QPR controller parameters can be found in reference [26-27].

4.1 | Load switching simulation

The simulation parameters of the dual micro-source system are shown in Table 2, and the feeder parameters of DG_3 are not included. The first simulation case is set as follows. the virtual resistances of two micro-sources are fixed to 0.09Ω at the initial time. The optimization process of virtual resistances is started at 0.5s and the public load of the system is increased by 0.1+j0.08MVA at 2s. The optimization process and hybrid indexes of virtual resistances are shown in Figure 9. The output power is shown in Figure 10. The second simulation case is set as follows. Virtual resistances of the two micro-sources is fixed to specific values. While 0.09Ω is chosen at random, 0.3Ω and 0Ω are selected based on circulation suppression. The index comparsion of simulation cases is shown in Table 3. The circulating current of random-selected resistances is taken as the denominator of I_h/% and the voltage allowable range, which is ±7% rated voltage, is taken as the denominator of U_v/%.

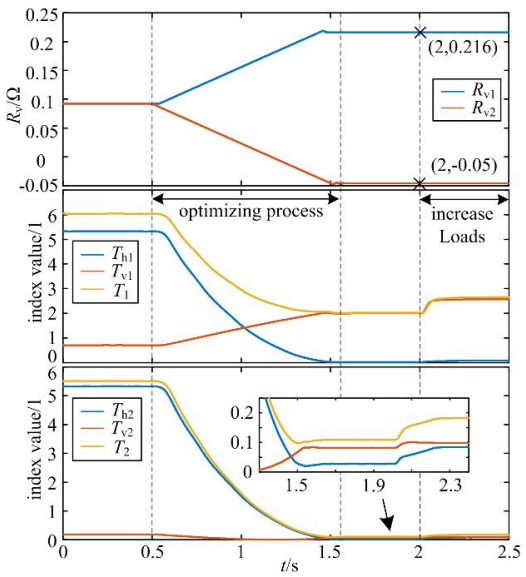

FIGURE 9 Diagram of virtual resistance and hybrid index during optimization

In Figure 9, the virtual resistances R_{v1} and R_{v2} iterate from 0.5s to 1.5s. During the iteration process, the virtual resistance R_{v1}, corresponding to R_{l1}, increases to 0.216Ω, whereas R_{v2} decreases to -0.05Ω. The hybrid

indexes T_1 and T_2 reduce to the equilibrium state. That is consistent with the analysis of the corresponding relationship between virtual resistance optimization and the hybrid index, which means the optimal values of virtual resistances correspond to the minimum points of hybrid indexes. It can be seen that, hybrid indexes change while virtual resistances are not optimized after the increase of the public load, which shows the change of the public load has little influence on the optimization results of the virtual resistance.

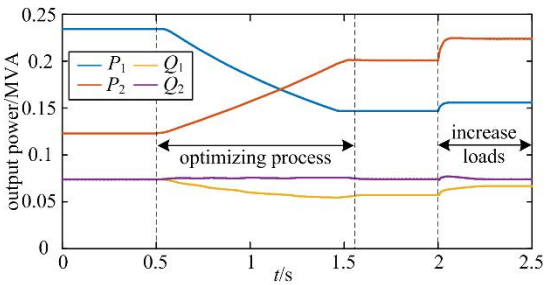

FIGURE 10 Diagram of output power during optimization

As shown in Figure 10, the deviation of output active powers is reduced from 0.11MW to 0.06MW with the same public load after virtual resistance optimization, which greatly improves the degree of active power sharing. The slight increase of reactive power deviation has little effect on the degree of reactive power sharing. Therefore, optimizing the virtual resistance can significantly improve the power sharing degree of the system and avoid the problem of long-term insufficient output power of some micro-sources.

Tab.3 Indexes comparison with different values of virtual resistances

	case1	case2	优化阻值
R_{v1}、R_{v2}/Ω	0.09、0.09	0.3、0	0.216、-0.05
I_h/kA	0.1032	0.001	0.0075
I_h/%	×	0.9%	7.2%
U_{v1}/kV	0.0076	0.0159	0.0131
U_{v1}/%	25%	51%	42%
U_{v2}/kV	0.0065	0	0.0048
U_{v2}/%	21%	0	16%

In Table 3, the first case is selected randomly, and its circulating current value is large, which easily causes power oscillation between inverters. It corresponding to Figure 10, the difference of active power output between the two micro-sources is 0.11MW, which shows the active power allocation is seriously unbalanced. In contrast, the second case and optimized resistance can greatly reduce the circulating current and improve the power sharing. However, the voltage deviation of the second case reaches 51%, and the voltage quality does not meet the requirements. It means the voltage quality must be increased with other methods, so the design of the second case is unreasonable. Comparing the second case with the optimized resistance, it is found that the the voltage quality is improved with optimized virtual resistance while the circulating current is greatly suppressed. Generally, virtual resistance optimization with the hybrid index can achieve the balance of suppressing circulation current and improve voltage quality, which is superior to other designs.

4.2 | DG switching simulation

The simulation parameters of three micro-sources system are shown in Table 2. The first simulation case is set as follows. the virtual resistances of all micro-sources are fixed to 0.115Ω at the initial time. The optimization process of virtual resistances is started at 0.5s and DG_3 quits running at 2.2 s, when the optimization iteration process is carried out again. The optimization process and hybrid indexes of virtual resistances are shown in Figure 11. The output power is shown in Figure 12. The second simulation case is set as follows. Virtual resistances of the three micro-sources is fixed to specific values, shown in Table 4. The first case is selected based on the improvement of voltage deviation and the second case is chosen at random, while the last two cases are selected based on circulation suppression. The index comparsion between the first case and the second case is shown in Table 5.

Tab.4 Values of virtual resistances without optimum design

	R_{v1}/Ω	R_{v2}/Ω	R_{v3}/Ω
case1	0	0	0
case2	0.115	0.115	0.115
case3	0.3	0	0.2
case4	0.1	-0.2	0

In Figure 11, the virtual resistances R_{v1}, R_{v2} and R_{v3} iterate from 0.5s to 1.5s for the first time. During the iteration process, the virtual resistance R_{v1} increases to 0.25Ω, while R_{v2} decreases to -0.045Ω. R_{v3} increases first and then decreases under the influence of the other two virtual resistances, and finally stabilizes at 0.14Ω.

The initial value of T_3 below the steady value indicates that the global optimum value is the result of the joint optimization of all virtual resistances rather than single local optimum value. The second iteration is the iteration process of R_{v1} and R_{v2} after DG_3 quits running.

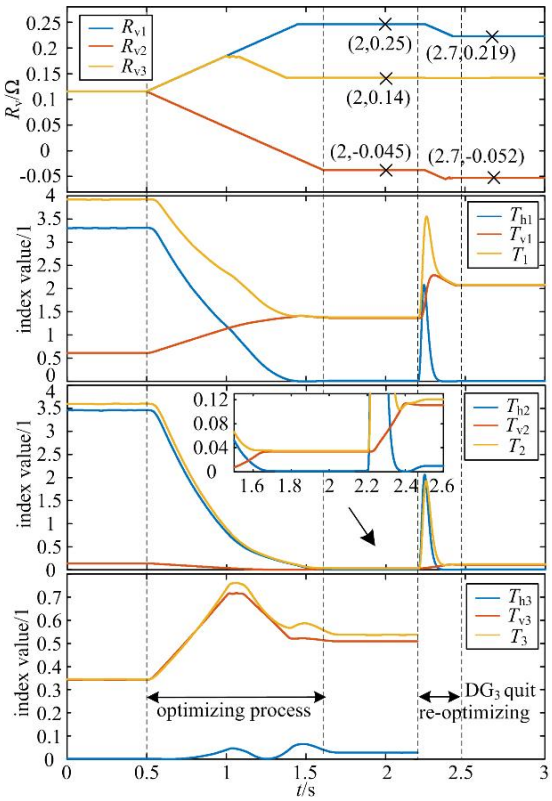

FIGURE 11 Diagram of virtual resistance and hybrid indexes during optimization

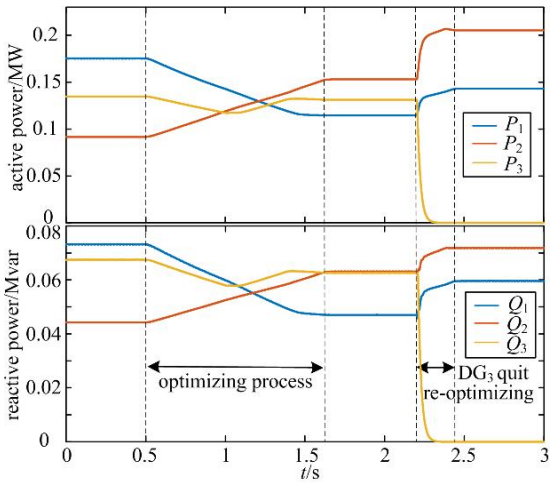

Fig. 12 Diagram of output power during optimization

After the first iteration, the virtual resistance is close to the optimal value, resulting in the second iteration process being very short, only 0.1s. After the first iteration, the virtual resistance is close to the optimum value, resulting in the second iteration process being very short, only 0.1s. The final stability values of R_{v1} and R_{v2} are 0.219Ω and -0.052Ω respectively, which are basically consistent with the results of virtual resistance optimization in Section 4.1. It shows that the results of virtual resistance optimization are affected by the number of micro-sources, but not by the switching process of micro-sources.

In Figure 12, the first iteration process significantly improves the power allocation of the system, while the second iteration does not significantly improve the power allocation because the quitting of DG_3 is equivalent to directly increasing the total public load. The improvement of reactive power equalization is more obvious than that of active power after DG_3 quits running. The reason is that the realization of active power equalization needs to satisfy the magnitude difference of output voltage among micro-sources in the low-voltage microgrid, which is more rigorous than the condition of realizing reactive power equalization. Generally, the optimization of virtual resistances can improve the power allocation of the system.

Tab.5 Indexes comparison with different values of virtual resistances

	I_{h1}/%	I_{h2}/%	I_{h3}/%	U_{v1}/%	U_{v2}/%	U_{v3}/%
case1	121.7	100	21.5	0	0	0
case2	79.8	81.6	1.8	29	14	21
case3	6.4	4.7	2	56	0	35
case4	1.6	1	0.1	21	-47	0
Optimi-zation	5.6	0.7	6.8	37	-8	26

In Table 5, the circulating currents of the first two cases are larger than that in other resistance values. The circulating currents of the third and fourth case are suppressed, but the voltage deviation does not meet the requirements and the power quality is poor. Generally, only optimizing resistance can improve power quality and obviously suppress the circulating current. It shows that optimizing virtual resistance based on the hybrid index is better than other schemes.

5 | Conclusion

In this paper, a virtual resistance optimization method based on the hybrid index is proposed. The hybrid index is defined with the circulating current level and voltage deviation, the optimization iteration process is designed

with the hybrid index as the objective function, and the constraints are deduced according to the power quality requirements, capacity constraints and static stability requirements. The main conclusions are as follows:

(1) The method of optimizing virtual resistance based on the hybrid index can achieve the effect of restraining circulating current and improving power sharing degree on the premise of guaranteeing power quality and satisfying system stability.

(2) The lower limit of virtual resistance can be obtained by analyzing power quality constraints and capacity constraints of inverters. The upper limit can be obtained by analyzing static stability, and the range of virtual resistance optimization can be determined by both.

(3) The optimization of virtual resistance is affected by the number of feeders. It is necessary to re-optimize the virtual resistance after changing the number of feeders, but the process of switching micro-source and adjusting load does not affect the optimized resistance value.

(4) In the process of virtual resistance optimization of multi-source system, There exists a hybrid index whose resistance value is lower than that of its optimal resistance value, which indicates that the optimization process is the process of all virtual resistors optimizing together.

Appendix

The simulation block diagram of the whole system is shown in Figure A_1.

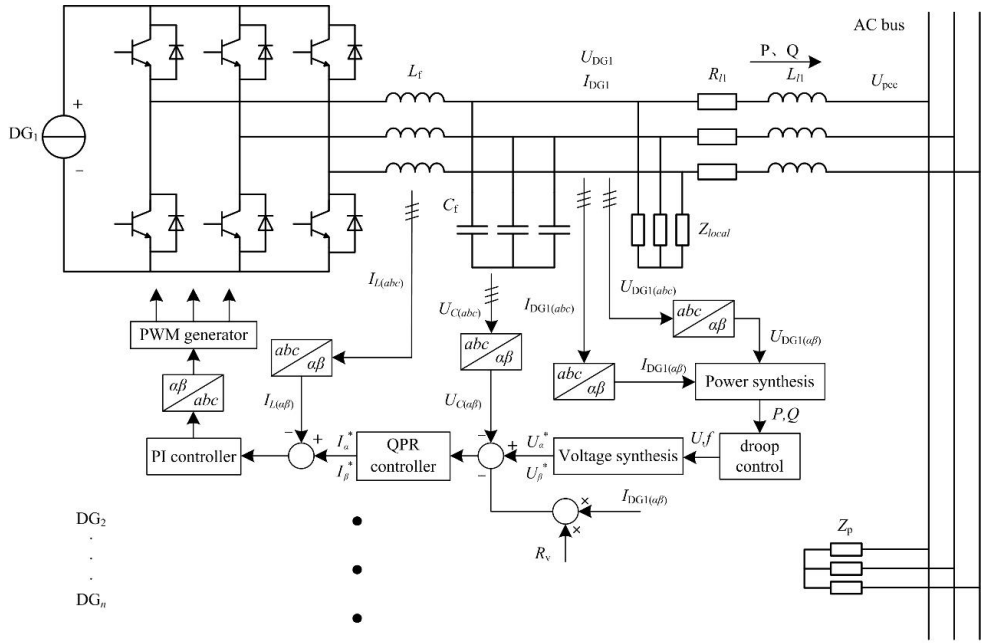

FIGURE A1 Diagram of low-voltage microgrid used for simulation

Reference

1. Shuai Z，Sun Y，John S，et al．Microgrid stability: Classification and a review[J] ． *Renewable and Sustainable Energy Reviews*，2016，58：167-179.
2. Claudio A C，Rodrigo P B，Daniel E. O，et al．Trends in Microgrid Control[J]．*IEEE Transactions on Smart Grid*，2014，5(4)：1905-1919.
3. Kim Y S，Kim E S，Moon S I．Distributed Generation Control Method for Active Power Sharing and Self-Frequency Recovery in an Islanded Microgrid[J]．*IEEE Transactions on Power Systems*，2016，32(1)：544-551
4. Zhu Yixin，Zhuo Fang，Wang Feng，et al．Virtual impedance optimization method for microgrid reactive power sharing control[J]．*Proceedings of the CSEE*，2016，36(17)：4552-4563.
5. Zhu G，Wei X，Lu J，et al．Instantaneous current-sharing control scheme of multi-inverter modules in parallel based on virtual circulating impedance[J]．*IET Power Electronics*，2016，9(5)：960-968.
6. Wen C，Huang Y，Hu C，et al．Adaptive Control of Virtual Impedance in Parallel Operation of Virtual Synchronous Generator Interface Converter[J]. *Transactions of China Electrotechnical Society*，2020，12(35)：494-502.
7. Ghanizdeh R，Gharehpetian G B．Voltage quality and load sharing improvement in islanded microgrids using distributed hierarchical control[J]．*IET Renewable Power Generation*，2019，13(15)：2888-2898.
8. Cai H，He X，Shi J，et al．Power decoupling strategy

based on ‘virtual negative resistor’ for inverters in low-voltage microgrids[J]. *IET Power Electronics*, 2016, 9(5): 1037-1044.

9. Hoang T V, Lee H H. An Adaptive Virtual Impedance Control Scheme to Eliminate the Reactive-Power-Sharing Errors in an Islanding Meshed Microgrid[J]. *IEEE Journal of Emerging & Selected Topics in Power Electronics*, 2018, 2(6): 966-976.
10. Han H, Hou X, Yang J, et al. Review of Power Sharing Control Strategies for Islanding Operation of AC Microgrids[J]. *IEEE Transactions on Smart Grid*, 2015, 7(1): 200-216.
11. Dou C, Zhang Z, Yue D, et al. Improved droop control based on virtual impedance and virtual power source in low-voltage microgrid[J]. *IET Generation Transmission & Distribution*, 2017, 11(4): 1046-1054.
12. Zhang H, Kim S, Sun Q, et al. Distributed adaptive virtual impedance control for accurate reactive power sharing based on consensus control in microgrids[J]. *IEEE Transactions on Smart Grid*, 2017, 8(4): 1749-1761.
13. Zhang Y, Yu M, Liu F, et al. Instantaneous Current-Sharing Control Strategy for Parallel Operation of UPS Modules Using Virtual Impedance[J]. *IEEE Transactions on Power Electronics*, 2013, 28(1): 432-440.
14. Liu Ruiming, Wang Shengtie. Power distribution of parallel converters in islanded microgrid using virtual resistance droop control[C]. 13th *IEEE Conference on Industrial Electronics and Applications*, Hubei, China, 2018.
15. Han Hua, Liu Yao, Sun Yao, et al. An Improved Control strategy for reactive power sharing in microgrids[J]. *Proceedings of the CSEE*, 2014, 34(16): 2639-2648.
16. Xia Y, Peng Y, Wei W. Triple droop control method for ac microgrids[J]. *IET Power Electronics*, 2017, 10(13): 1705-1713.
17. Chen Y, Josep M G, Shuai Z, et al. Fast Reactive Power Sharing, Circulating Current and Resonance Suppression for Parallel Inverters Using Resistive-Capacitive Output Impedance[J]. *IEEE Transactions on Power Electronics*, 2016, 31(8): 5524-5537
18. Augustine S, Mishra M K, Lakshminarasamma N. Adaptive droop control strategy for load sharing and circulating current minimization in low-voltage standalone DC microgrid[J]. *IEEE Transactions on Sustainable Energy*, 2015, 6(1): 132-141.
19. Peng Z, Wang J, D B, et al. The Application of Microgrids Based on Droop Control With Coupling Compensation and Inertia[J]. *IEEE Transactions on Sustainable Energy*, 2018, 3(9): 1157-1168.
20. Wang Y, Yang G, Zhuang J, et al. Zero-Error Frequency Regulation Control Method for Microgrids Based on Consensus Algorithm[J]. *Electric Power*, 2020, 53(10): 5.
21. Wu L, Liu Q, Tang C, et al. Design of secondary frequency/voltage controller with feedback linearization and distributed implemention in microgrids[J]. *Power System Protection and Control*, 2019, 47(14): 8.
22. Shafiee Q, Guerrero J M Vasquez J C. Distributed secondary control for islanded microgrids — a novel approach[J]. *IEEE Transactions on Power Electronics*, 2013, 29(2): 1018-1031.
23. He J, Li Y W, Blaabjerg F. An Enhanced Islanding Microgrid Reactive Power, Imbalance Power, and Harmonic Power Sharing Scheme[J]. *IEEE Transactions on Power Electronics*, 2015, 30(6): 3389-3401.
24. Xuan Z, Jia W, Jing H, et al. Research on three-phase grid-connected inverter filter[J]. *Mechanical Engineering & Automation*, 2018. 2(4): 24-28.
25. Liu R, Wang S. Power distribution of parallel converters in islanded microgrid using virtual resistance droop control[C]. 13th *IEEE Conference on Industrial Electronics and Applications*, Hubei, China, 2018.
26. Cha H, Vu T K, Kim J E. Design and control of Proportional-Resonant controller based Photovoltaic power conditioning system[C]. *Energy Conversion Congress and Exposition*, 2009.
27. Huang Ruhai, Xie Shaojun. Double-loop digital control strategy based on proportional-resonant controller[J]. *Transactions of China Electrotechnical Society*, 2014, 27(2): 77-81.